does not contradict the structure image and the crystal structure given by Toman & Frueh (1973).

It is generally known that both the orientation and the spacing of satellites in X-ray and electron diffraction patterns vary with chemical composition of the plagioclase. The cause is attributable to the antiphase structure owing to the alternation of Ca/Na occupancy. For a specimen of An50, no Na-rich or Ca-rich regions exist (Kumao, Hashimoto, Nissen & Endoh, 1981). In a specimen of An67, it has been found that Ca-rich or anorthite-like regions exist along the antiphase boundaries in the form of thin layers. The thickness of the layers is assumed to increase with Ca content. For compositions containing less Ca than An50, Na-rich or albite-like regions may occur along the boundaries (Nissen, 1982). Thus, the superstructure of plagioclase feldspar probably consists of three basic structures, *i.e.* the albite-like, the labradorite-like and the anorthite-like structure.

The authors are indebted to Professor H. Hashimoto, Okayama University of Science, for valuable discussions and encouragement, and to Dr J. Ylä-Yääski for his help in the computation work. Part of this work was supported by the Swiss National Science Foundation.

References

BAMBAUER, H. U., EBERHARD, E. & VISWANATHAN, K. (1967). *Schweiz. Mineral. Petrogr. Mitt.* 47, 351-364.

CHAO, S. H. & TAYLOR, W. H. (1940). *Proc. R. Soc. London Ser. A*, **176**, 76-87.

COWLEY, J. M. & MOODIE, A. F. (1957). *Acta Cryst.* **10**, 609-619.

HASHIMOTO, H., KUMAO, A., ENDOH, H., NISSEN, H.-U., ONO, A. & WATANABE, E. (1975). *Proceedings of the EMAG Conference, Bristol*, pp. 245-250.

HORST, W., TAGAI, T., KOREKAWA, M. & JAGODZINSKI, H. (1981). *Z. Kristallogr.* **157**, 233-250.

JAGODZINSKI, H. & KOREKAWA, M. (1976). *Z. Kristallogr.* **143**, 239-277.

JAGODZINSKI, H. & KOREKAWA, M. (1978). *Phys. Chem. Miner.* **3**, 69-72.

KITAMURA, M. & MORIMOTO, N. (1977). *Phys. Chem. Miner.* **1**, 199-212.

KOREKAWA, M. & HORST, W. (1974). *Fortschr. Mineral.* **52**, 37-40.

KOREKAWA, M., HORST, W. & TAGAI, T. (1978). *Phys. Chem. Miner.* **3**, 74-75.

KOREKAWA, M. & JAGODZINSKI, H. (1967). *Schweiz. Mineral. Petrogr. Mitt.* **47**, 269-278.

KUMAO, A., HASHIMOTO, H., NISSEN, H.-U. & ENDOH, H. (1981). *Acta Cryst.* A**37**, 229-238.

LIPSON, H. & MICHAEL, W. S. (1974). *J. Appl. Cryst.* **7**, 577-585.

NAKAJIMA, Y., MORIMOTO, N. & KITAMURA, M. (1977). *Phys. Chem. Miner.* **1**, 213-225.

NISSEN, H.-U. (1974). *The Feldspars*, edited by W. S. MACKENZIE & J. ZUSSMAN, pp. 491-521. Manchester Univ. Press.

NISSEN, H.-U. (1982). Report presented at the Autumn Meeting of Schweiz. Mineral. Petrog. Ses., Bern.

SKARNULIS, A. J. (1979). *J. Appl. Cryst.* **12**, 636-638.

TAGAI, T., JOSWIG, W., KOREKAWA, M. & WENK, H.-R. (1980). *Z. Kristallogr.* **151**, 77-89.

TANJI, T. & HASHIMOTO, H. (1978). *Acta Cryst.* A**34**, 453-459.

TOMAN, K. & FRUEH, A. J. (1973). *Z. Kristallogr.* **138**, 337-342.

TOMAN, K. & FRUEH, A. J. (1976). *Acta Cryst.* B**32**, 521-525, 526-538.

Acta Cryst. (1987). B**43**, 333-343

The Electron Density Distribution in Calcium Metaborate, $Ca(BO_2)_2$

BY A. KIRFEL

Mineralogisches Institut der Universität Bonn, Lehrstuhl für Mineralogie und Kristallographie, Poppelsdorfer Schloss, D-5300 Bonn 1, Federal Republic of Germany

(*Received* 24 *August* 1986; *accepted* 16 *March* 1987)

Abstract

The room-temperature electron density distribution in $Ca(BO_2)_2$ has been studied by X-ray diffraction experiments on two crystals, I and II, up to $s = (\sin\theta)/\lambda = 0{\cdot}80$ and $1{\cdot}16$ Å^{-1}, respectively. Conventional structure refinements yielded $wR = 0{\cdot}025/0{\cdot}021$ for 603/1577 observed reflections. Data set II was used for high-order refinements with varying cut-offs in order to assess positional and thermal parameters least biased by bonding effects and to estimate a 'best' scale factor. Rigid pseudoatom multipole expansions up to hexadecapoles resulted in final agreement factors $wR = 0{\cdot}0064/0{\cdot}0088$ which represent highly significant improvements of the fit with observations. Parameters derived from the multipole refinements of both data sets I and II were used to calculate dynamic and static deformation density distributions and deformation potential distributions in interesting sections of the structure. The choice of the resolution of the Fourier synthesis is shown to affect $\Delta\rho(\mathbf{r})$, especially around the nuclear positions. The observed charge distributions are discussed in terms of chemical bonding in $Ca(BO_2)_2$ and in comparison with an earlier study on $LiBO_2$. In addition, spherical-charge integrations around Ca and B served to establish formal ionic radii and charges of the cations. All relevant results indicate a predominantly ionic interaction between Ca^{2+} and the $(BO_2)^-$ anions (of metaboric acid) which polymerize to endless chains of

0108-7681/87/040333-11$01.50

BO_3 triangles. [Crystal data: $M_r = 125{\cdot}70$, space group *Pnca*, $a = 6{\cdot}2046\,(3)$, $b = 11{\cdot}5865\,(7)$, $c = 4{\cdot}2747\,(3)$ Å, $V = 307{\cdot}31\,(6)$ Å^3, $Z = 4$.]

Introduction

In a previous paper (Kirfel, Will & Stewart, 1983), the chemical bonding in lithium metaborate, $LiBO_2$, was elucidated by a thorough electron density study. A simple model of binding in the molecular unit $LiBO_2$ and in the crystal was derived by comparing features of the experimental deformation density distribution with calculated diatomic deformation densities, especially with that of Li–O. The results indicated that the fourfold-coordinated Li atom forms one preferred bond with the terminal O atom of the BO_3 triangle which is the basic unit of endless chains $[BO_2]_\infty^{-\infty}$. In continuation of this work, a comparative study on calcium metaborate, $Ca(BO_2)_2$, was carried out with the results reported below.

The crystal structure of $Ca(BO_2)_2$ was investigated as early as 1932 (Zachariasen & Ziegler, 1932). A later detailed study with 217 reflections resulting in $R = 0{\cdot}038$ is due to Marezio, Plettinger & Zachariasen (1963). Crystals are orthorhombic with space-group symmetry No. 60, *Pnca*, $Z = 4$. The structure (Fig. 1) contains endless chains $[BO_2]_\infty^{-\infty}$ of BO_3 triangles. The chains run along **c** and form layers parallel to (010); the atoms within a chain are almost coplanar, and approximately parallel to (100). Thus, the arrangement of the chains is similar to that found in $LiBO_2$. The Ca atom lies between four chains on a twofold axis $(\frac{1}{4}, 0, z)$, and is (in contrast to $LiBO_2$) eightfold coordinated by O atoms with four unique Ca–O distances varying from 2·3396 to 2·7126 Å. Three of them connect Ca to one chain, while the shortest bond provides the link to a second chain (Fig. 1*a*). Thus, each of the Ca atoms, which themselves form zig-zag chains in planes parallel to (010), is connected with four $[BO_2]_\infty^{-\infty}$ chains. The coordination polyhedron CaO_8 is shown in Fig. 1(*b*). The O atoms form a distorted cube of symmetry 2 with O–O edge lengths between 2·3205 and 3·2558 Å. The two short edges are identical to the edges of BO_3 triangles, O(1)–O(2), of two chains.

In comparison with $LiBO_2$ one finds, therefore:

(i) similar arrangement of B and O atoms, *e.g.* of chains of BO_3 triangles;

(ii) a different coordination of the cation connecting the chains.

Consequently, the deformation density in $Ca(BO_2)_2$ can be studied under two aspects: (1) to obtain insight into the chemical bonding (atomic interactions, formal atomic charges); and (2) to compare quantitatively deformation density features with results for $LiBO_2$. Aspect (2) should shed more light on the reliability and replicability of charge density studies by conventional X-ray diffraction techniques.

The suitability of $Ca(BO_2)_2$ for such a study can be estimated from (Stevens & Coppens, 1976)

$$S = V(Z \sum n_{\text{core}}^2)^{-1} = 0{\cdot}22. \qquad (1)$$

This number is about ten times smaller than that for $LiBO_2$. However, significant charge redistributions due to chemical bonding may still be observable, as has been the case in Mg_2SiO_4 ($S = 0{\cdot}23$; van der Wal, Vos & Kirfel, 1987), $(Ca,Mg)(CO_3)_2$ ($S = 0{\cdot}23$; Effenberger, Kirfel & Will, 1983) and $CaSO_4$ ($S = 0{\cdot}17$; Kirfel & Will, 1980, 1981). Finally, $Ca(BO_2)_2$ also possesses a high melting point of 1427 K which precludes the necessity of employing low temperatures. Moreover, the centrosymmetry excludes problems due to model-dependent phasing of the structure amplitudes.

Experimental

Colourless needle-shaped crystals obtained from the melt were kindly provided by Behm (1976). For the X-ray diffraction experiments, two samples were selected and checked for good quality by Weissenberg

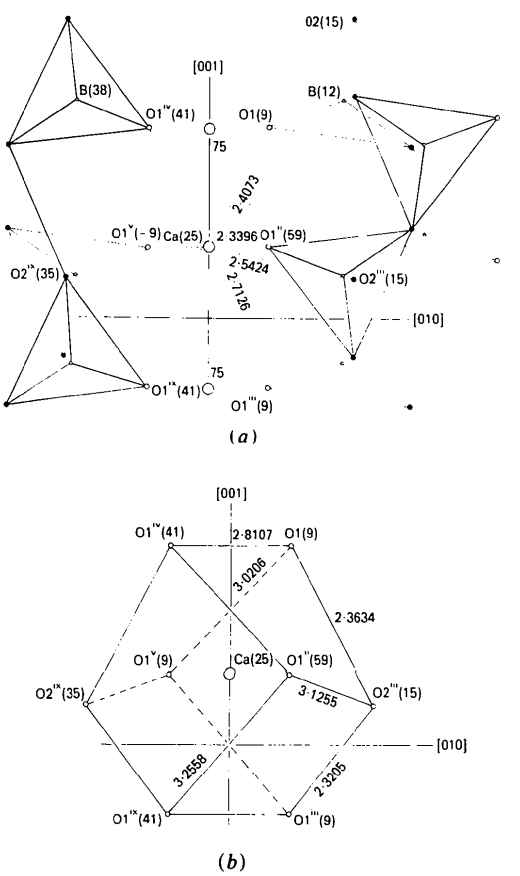

Fig. 1. (*a*) Projection of the structure along [100]. In parentheses *x* coordinates (×100); numbering scheme of atoms according to symmetry code of Table 6. (*b*) The Ca coordination polyhedron viewed along [100].

photographs. Diffraction data were collected on an automatic four-circle diffractometer (Syntex $P2_1$) with Mo $K\alpha$ radiation monochromatized by a graphite crystal ($2\theta_m = 12{\cdot}2°$).

The unit-cell parameters were determined for crystal II by least squares from the 2θ settings of 37 independent reflections in the range $56 < 2\theta < 64°$ [λ(Mo $K\alpha_1$) = 0·70926 Å]. Each reflection was measured twice, *i.e.* at $\pm 2\theta$.

For the data collection, the total background counting time equalled the time spent for the peak count. Data reduction was carried out by (i) adjusting the intensities to the fluctuations of the sums of the check reflection intensities, (ii) empirical absorption correction using ψ-scan intensities of some 40 reflections equally distributed over the investigated 2θ range, (iii) Lp correction, and (iv) averaging of symmetry-equivalent reflections. In the latter procedure $I(\mathbf{h})$ and $\sigma(I)$ were calculated according to

$$\overline{I(\mathbf{h})} = \frac{\sum I(\mathbf{h})_i / \mathrm{var}\,[I(\mathbf{h})_i]_{\mathrm{count}}}{\sum 1/\mathrm{var}\,[I(\mathbf{h})_i]_{\mathrm{count}}}, \quad (2)$$

$$\sigma[I(\mathbf{h})] = \left\{ \frac{[\overline{I(\mathbf{h})} - I(\mathbf{h})_i]^2}{2(N-1)} + \frac{\sum \mathrm{var}\,[I(\mathbf{h})]_{\mathrm{count}}}{2N} \right\}^{1/2}, \quad (3)$$

where N = number of contributing reflections.

Thus, the $\sigma(I)$ were estimated as the means of both scatter of equivalent reflections and counting statistics. The ensuing total internal agreement factor of the data is defined as

$$R(I)_{\mathrm{int}} = \sum_j \sum_i |\bar{I}_j - I_{ji}| / \sum \sum I_{ji}. \quad (4)$$

Finally, structure amplitudes $|F(\mathbf{h})|$ were calculated and flagged as unobserved for $|F| < FAK\,\sigma(F)$.

Crystallographic data for $Ca(BO_2)_2$ and details of the data collection and processing are given in Tables 1 and 2. The agreement between the two data sets was assessed by scaling data set I onto data set II using the sums of all corresponding $F(h)_o$, and calculating an agreement factor $R(|F|)_{\mathrm{int}} = \sum |\Delta F(\mathbf{h})| / \sum |F(\mathbf{h})| = 0{\cdot}0068$ (0·0090 including unobserved data). These figures indicate close agreement between the two sets, and merging of the sets was therefore considered unnecessary.*

Table 1. *Crystallographic data for* $Ca(BO_2)_2$

	This work	Marezio *et al.* (1963)
a_0 (Å)	6·2046 (3)	6·214 (3)
b_0	11·5865 (7)	11·604 (4)
c_0	4·2747 (3)	4·285 (1)
V (Å^3)	307·31 (6)	308·98
Space group	*Pnca*	*Pnca*
M_r (g mol^{-1})	125·70	
Z	4	
D_x (Mg m^{-3})	2·715	
μ(Mo $K\alpha$) (mm^{-1})	1·73	

Table 2. *Data collection and processing*

	Crystal I	Crystal II
Wavelength (Å)	0·71069	
Crystal dimensions (mm)	0·2 × 0·2 × 0·3	0·2 × 0·25 × 0·3
$[(\sin\theta)/\lambda]_{\max}$ (Å^{-1})	0·807	1·153
Scan mode	θ–2θ step scan	
Steps/reflection	96	
Scan angle (°)	2·0 plus (α_1, α_2)	
Scan speed (° min^{-1})	1·0–10.0	
hkl range	Full sphere	$0 < 2\theta \le 80°$ full $80 < 2\theta \le 110°$ half
Number of check reflections	3 (311, 151, 0, 10, 0)	
Monitor interval	31	
Long-term oscillations of $\sum I_{\mathrm{check}}$	1·0–1·11	1·0–1·06
Number of reflections recorded	5404	11565
Number of unique reflections	670	1938
Number of unobserved reflections [$\lvert F\rvert < FAK\,\sigma(F)$]	67	361
FAK	1·5	2·0
$R(I)_{\mathrm{int}}$ (without absorption correction)	0·0254	
$R(I)_{\mathrm{int}}$ (after absorption correction)	0·016	0·024

Data analysis

(*a*) *Independent-atom model* (IAM) *refinements*

The positional and thermal parameters reported by Marezio *et al.* (1963) were taken as starting values for conventional independent-atom (IAM) structure refinements on $|F|$ using all data, with weights $w = 1/\sigma^2(F)$.

Scattering factors were calculated for neutral atoms B, O, Ca as well as for Ca^{2+} from the Hartree–Fock (HF) wave functions given by Clementi & Roetti (1974). Anomalous-dispersion factors were taken from Cromer & Liberman (1970), and extinction was corrected by including an isotropic extinction coefficient (Becker & Coppens, 1974) in the refinement. For crystal II, several high-order (HO) refinements with increasing cut-off angles were carried out in order to obtain a set of standard parameters least biased by bonding effects. These refinements were also used to establish a 'best' scale-factor estimate which could be applied to both data sets prior to the multipole refinements.

The results of the various IAM refinements can be summarized briefly as follows.

(i) For each of the data sets I and II, the parameters resulting from the all-data refinements using Ca or Ca^{2+}, respectively, did not differ significantly. Therefore, Tables 4 and 5 show only parameters from the all-data refinement of set I (Ca^{2+}) and from the best HO refinement ($s_{\min} = 0{\cdot}7$ Å^{-1}) of set II (Ca), for

* A list of observed structure factors and e.s.d.'s for crystal II has been deposited with the British Library Document Supply Centre as Supplementary Publication No. SUP 43815 (14 pp.). Copies may be obtained through The Executive Secretary, International Union of Crystallography, 5 Abbey Square, Chester CH1 2HU, England.

comparison with the multipole results. A survey of these two sets of parameters shows significant variations of both the positional and thermal parameters which are attributable to bonding-electron contributions to the LO-structure amplitudes not included in II (Ca, HO07). The better fit of the spherical-atom model to the HO data of crystal II is also demonstrated by the decrease of the R values from $R = 0{\cdot}019$, $wR = 0{\cdot}021$ (all data) to $R = 0{\cdot}0166$, $wR = 0{\cdot}0126$ (HO07).

(ii) For both data sets, several isotropic-extinction corrections were tested assuming type 1 or 2 models with Gaussian or Lorentzian distribution. They all yielded practically identical results with marginal preference for a type-2 correction with Lorentzian distribution. This type of correction was used in all ensuing refinements. For most reflections, extinction effects were small. For (I) only seven and for (II) six reflection correction factors $Y^{1/2}$ were smaller than 0·98; the two reflections most affected by extinction were 020 [$Y^{1/2} = 0{\cdot}93$ (I), 0·94 (II)] and 210 [$Y^{1/2} = 0{\cdot}94$ (I), 0·96 (II)].

(iii) Scale-factor–temperature-factor correlations increased in the HO refinements beyond the 0·7 Å^{-1} cut-off. Simultaneously, the R values increased due to the decreasing quality of observations, and therefore the scale factor derived from HO07 (1·029) was regarded as the best estimate of the absolute scale and applied to the data. However, experience gained from many electron density studies based on relative intensities shows that an uncertainty of about 1% has still to be taken into account in the preparation and interpretation of deformation density maps.

(*b*) *Multipole refinements*

Full-angle multipole refinements have been carried out for both data sets I and II, using either neutral atoms Ca, B and O (model Ca), or alternatively Ca^{2+}, B and O (model Ca^{2+}).

In the program *VALRAY* (Stewart, 1976; Stewart & Spackman, 1981), the total density in the asymmetric unit is assumed to be the sum of localized pseudoatom densities ρ^{at}. The density with respect to its nucleus of each pseudoatom p is given by

$$\rho_p(\mathbf{r}_p) = \mathrm{Pop}_p^{sph}\rho_p^{sph}(r_p) + \Delta\rho_p(\mathbf{r}_p) \qquad (5)$$

with

$$\Delta\rho_p(\mathbf{r}_p) = \sum_l \sum_{m=0}^{l} [\sum_i \mathrm{Pop}_p(l,m,i)\rho_p(l,i,r_p)]\, Y_{lm\pm}(\theta,\varphi). \qquad (6)$$

r_p, θ and φ are polar coordinates of $\mathbf{r}_p$; $Y_{lm\pm}(\theta,\varphi)$ are Tesseral harmonics; and $\rho_p^{sph}(r_p)$ is the conventional independent-atom density represented by HF scattering factors deduced from the wave functions (Clementi & Roetti, 1974) for neutral or charged atoms. The index i in (6) indicates the option of using more than one radial deformation function per multipole order. The radial distribution functions $\rho_p(l, r_p)$ are chosen as single exponential functions (SEF's) of the type

$$r^n \exp(-\alpha_{p,1} r_p) \text{ with } n \geq 1. \qquad (7)$$

Each pseudoatom is considered to be a rigid entity, and therefore the thermal motion is taken to be the same for all multipole functions assigned to the atom.

Table 3. *Details of the multipole refinements of I and II*

Least-squares function minimized		$Q = \sum_{\mathbf{h}} w[\lvert F_o(\mathbf{h})\rvert - \lvert F_c(\mathbf{h})\rvert Y^{1/2}(\mathbf{h})]^2$					
$\lvert F_o\rvert$ weights		$w = [\sigma(\lvert F_o\rvert)]^{-2}$					
f^{sph}		Clementi & Roetti (1974) Model (Ca): Ca, B, O Model (Ca^{2+}): Ca^{2+}, B, O					
Anomalous dispersion		Cromer & Liberman (1970)					
Extinction		Isotropic, type 2, Lorentzian mosaic spread					
Deformation functions		SEF of type $r^n \exp(-\alpha_1 r)$ normalized to 1 electron for $l \neq 0$; two monopoles ($i = 1, 2$) per atom					
l values (i for $l = 0$)		0 (1)	0 (2)	1	2	3	4
Constraints:							
Ca	n	$4^I, 3^{II}$	2	2	2	3	4
	α_1	3·5					
Ca^{2+}	n	$4^I, 2^{II}$	$2^I, 3^{II}$	2	2	3	4
	α_1	3·5					
B	n	3	2	2	2	3	4
	α_1	3·0*					
O	n	3	2	2	2	3	4
	α_1	4·5*					
		$\alpha[0; O(1)] = \alpha[0; O(2)]$					
Pop's		Pop(sph; Ca) = 20; Pop(sph; Ca^{2+}) = 18 Pop(sph; B) = 5; Pop(sph; O) = 8					

* $\alpha = 2\xi$, ξ being the standard molecular parameter of Hehre, Ditchfield, Stewart & Pople (1970).

Details of the refinements are summarized in Table 3 showing that each atom was assigned two monopoles, one with a fixed α_0. All other α_1 were treated as variables.

Although extinction effects were small in the IAM refinements, correlation of the extinction parameter with the parameters of the deformation functions, and in particular with the α's, was important. Therefore, the extinction correction factors obtained from the all-data refinements were kept constant throughout the multipole refinements. These were carried out with crystallographic standard parameters and multipole parameters in alternating cycles. This procedure yields convergence of the rather flexible multiple model. However, it leads necessarily to underestimation of the standard deviations.

(*c*) *Results of the refinement*

Agreement factors of all multipole refinements (Table 4) and Hamilton's (1965) test indicate a highly significant improvement of the fit with the observations. According to the R values, models using neutral Ca and ionic Ca^{2+} are equally acceptable. Results for the positional and thermal parameters are listed in

Table 4. *Fractional coordinates* ($\times 10^5$) *with e.s.d.'s in parentheses and agreement factors*

		IAM refinements		Multipole refinements			
		I(Ca^{2+})	II(Ca, HO07)	I(Ca^{2+})	I(Ca)	II(Ca^{2+})	II(Ca)
Ca	z	27214 (4)	27231 (2)	27234 (2)	27231 (1)	27231 (1)	27231 (1)
B	x	12528 (16)	12553 (4)	12548 (4)	12557 (4)	12550 (3)	12549 (3)
	y	19233 (7)	19253 (2)	19248 (2)	19255 (2)	19253 (2)	19253 (2)
	z	82886 (20)	82925 (5)	82934 (5)	82945 (6)	82924 (4)	82920 (4)
O(1)	x	9109 (10)	9090 (3)	9073 (3)	9083 (3)	9087 (2)	9088 (2)
	y	8628 (4)	8632 (2)	8630 (2)	8633 (2)	8623 (1)	8632 (1)
	z	72921 (13)	72949 (4)	72943 (3)	72955 (5)	72953 (3)	72952 (3)
O(2)	x	14831 (11)	14867 (4)	14882 (3)	14876 (4)	14863 (2)	14862 (2)
	y	20786 (4)	20788 (2)	20785 (2)	20789 (2)	20796 (1)	20797 (1)
	z	115249 (14)	115268 (3)	115300 (3)	115291 (4)	115251 (3)	115253 (3)
*NR**		670	1499	670	670	1938	1938
*NP**		34	33	143	143	143	143
R		0·0184	0·0166	0·0072	0·0073	0·0114	0·0114
wR		0·0250	0·0126	0·0064	0·0065	0·0088	0·0088
GOF		4·0	1·08	1·04	1·02	0·94	0·96

* *NR* = number of reflections (including unobserved); *NP* = number of variables.

Table 5. *Thermal parameters* U_{ij} ($Å^2 \times 10^5$) *with e.s.d.'s in parentheses*

		IAM refinements		Multipole refinements			
		I(Ca^{2+})	II(Ca, HO07)	I(Ca^{2+})	I(Ca)	II(Ca^{2+})	II(Ca)
Ca	U_{11}	910 (9)	813 (2)	819 (2)	844 (2)	815 (1)	827 (1)
	U_{22}	722 (6)	691 (2)	705 (2)	724 (2)	669 (2)	677 (2)
	U_{33}	920 (8)	825 (2)	837 (2)	859 (2)	797 (2)	807 (2)
	U_{12}	−70 (6)	−74 (2)	−74 (2)	−69 (2)	−73 (2)	−72 (2)
B	U_{11}	1065 (35)	1160 (7)	1326 (9)	1213 (9)	1186 (6)	1194 (6)
	U_{22}	824 (28)	627 (6)	578 (8)	608 (9)	604 (5)	606 (4)
	U_{33}	770 (29)	572 (6)	552 (8)	631 (9)	554 (4)	554 (4)
	U_{12}	28 (30)	−10 (6)	−36 (6)	−32 (6)	−14 (4)	−15 (4)
	U_{23}	−39 (28)	−28 (6)	−59 (7)	−44 (7)	−24 (4)	−25 (4)
	U_{13}	−11 (24)	−17 (5)	−40 (6)	−41 (7)	−23 (3)	−25 (4)
O(1)	U_{11}	1181 (23)	1201 (5)	1185 (6)	1222 (6)	1214 (3)	1211 (3)
	U_{22}	792 (20)	664 (3)	686 (6)	723 (6)	658 (3)	651 (3)
	U_{33}	1079 (23)	975 (4)	999 (6)	976 (6)	945 (3)	943 (3)
	U_{12}	−112 (20)	−163 (3)	−159 (5)	−151 (5)	−166 (3)	−167 (3)
	U_{13}	127 (20)	132 (4)	131 (5)	139 (5)	126 (3)	124 (3)
	U_{23}	−162 (21)	−194 (3)	−212 (5)	−195 (5)	−189 (3)	−189 (3)
O(2)	U_{11}	2334 (42)	2451 (9)	2387 (8)	2482 (8)	2458 (6)	2460 (6)
	U_{22}	781 (20)	693 (4)	681 (6)	731 (6)	680 (3)	682 (3)
	U_{33}	638 (20)	498 (4)	541 (6)	511 (6)	491 (3)	494 (3)
	U_{12}	212 (20)	240 (5)	233 (6)	239 (6)	238 (4)	237 (4)
	U_{13}	−158 (21)	−125 (5)	−126 (6)	−123 (6)	−125 (4)	−124 (3)
	U_{23}	−10 (20)	−47 (5)	−59 (5)	−60 (5)	−51 (3)	−50 (3)

Tables 4 and 5. They are in the following discussed in terms of the overall agreement with the IAM results II (HO07).

(i) The r.m.s. deviations of the positional parameters from II (HO07) in units of $Å \times 10^4$ are 14 for the IAM refinement I(Ca^{2+}) and 7, 5, 4 and 4 for the multipole refinements I(Ca^{2+}), I(Ca), II(Ca^{2+}) and II(Ca), respectively. These r.m.s. figures demonstrate the good agreement between HO and multipole results, particularly for set II where the differences d in Å are well below 0·001 Å with the exception of $d[y(O2)] = 0{\cdot}001$ Å. Differences between I(Ca^{2+}) and II(HO07) are considerably larger {*e.g.* $d[y(B)] = 0{\cdot}0023$, $d[x(O2)] = 0{\cdot}0022$ Å}, indicating significant bias in the IAM positions.

(ii) As to the vibrational parameters, r.m.s. deviations are (in units of $Å^2 \times 10^4$): 9, 4·3, 2·8, 1·35 and 1·4 for I(Ca^{2+}; IAM), I(Ca^{2+}), I(Ca), II(Ca^{2+}) and II(Ca), respectively. The U_{ij} of the IAM refinement of the limited data set I are strongly biased, showing on average too large vibrations normal to **a** and too small vibrations along **a**. Since the BO_3 triangles are roughly perpendicular to **a**, it is tempting to conclude that this effect is due to the bonding electron density in the triangle.

The agreement between the thermal parameters obtained from II(HO07) and the II multipole refinements is in the range of the average of their e.s.d.'s ($1{\cdot}0$–$1{\cdot}5 \times 10^{-4}$ $Å^2$) indicating a successful separation of thermal smearing and bonding effects in these refinements, at least for the B and O atoms. This may not be the case for the multipole refinements of set I. However, these still yield results superior to the IAM refinement in spite of the limited resolution.

For the Ca atom, the principal U_{ii} are (*a*) smaller using Ca^{2+} instead of Ca, and (*b*) smaller for data set II than for set I. Result (*a*) has to be attributed to a correlation between the temperature factors and the monopole functions assigned to Ca. Result (*b*) can be ascribed to the difference in resolution. Since U_{22} and U_{33} from II(Ca^{2+}, Ca) are also lower than corresponding values from II(HO07), one may suspect that the deformation density effects (see below) and thermal motion were not completely separated.

Calculation of deformation densities and potentials

With the positional and thermal parameters from the multipole refinements, Fourier maps of interesting sections were calculated according to Stewart (1979). The dynamic deformation density is defined as

$$\Delta\rho_{\rm dyn}(\mathbf{r}) = (2/V)\sum \Delta F(\mathbf{h}) \cos 2\pi\mathbf{hr} \qquad (8)$$

with

$$\Delta F(\mathbf{h}) = [K\,|F(\mathbf{h})_o| - |F(\mathbf{h})_c^{\rm IAM}|] \exp[i\Phi(\mathbf{h})_c^{\rm mult}]. \qquad (9)$$

From all $\Delta\rho_{\rm dyn}$ maps of models containing Ca^{2+} ions a constant term $8/V_{\rm cell}$ e Å^{-3} was subtracted in order to account for the contribution of $F(000)$.

The static deformation density is obtained directly from direct-space calculations according to

$$\Delta\rho_{\rm stat}(\mathbf{r}) = \sum_{\rm sym}\sum_{p}[\rho(\mathbf{r}-\mathbf{r}_p) - \rho(|\mathbf{r}-\mathbf{r}_p|)_p^{\rm IAM}], \qquad (10)$$

where $\rho(\mathbf{r}-\mathbf{r}_p)_p$ is a pseudoatom density and $\rho(|\mathbf{r}-\mathbf{r}_p|)_p^{\rm IAM}$ is the IAM density at site *p*.

The dynamic deformation potential $\Delta\psi(\mathbf{r})$ is calculated by Fourier summation with coefficients $-4\pi\{\Delta F(\mathbf{h})[(\sin\theta)/\lambda]^{-2}\}$. Since this calculation requires a neutral unit cell, only model II(Ca) has been considered. Negative regions in $\Delta\psi(\mathbf{r})$ indicate bond-induced lowering of the potential with respect to the independent-atom model, and the distribution can well be employed in characterizing the most stable parts in the structure.

Results

In order to assess the influence of resolution and scale factor on the dynamic deformation density distribution, the linear deformation density along B–O(1) was calculated for II(Ca) using reflections up to $[(\sin\theta)/\lambda]_{\rm max} = 0{\cdot}8$, $1{\cdot}0$ and $1{\cdot}16$ Å^{-1}, respectively.

In each case two scale factors were applied, $K = 1{\cdot}0$ and $K = 0{\cdot}99$. Results are shown in Fig. 2. As is well known, changing K in (9) by only 1% affects $\Delta\rho_{\rm dyn}(\mathbf{r})$ considerably near the atomic sites.

It is common practice to limit Fourier syntheses of deformation densities to data with, say, $s < 0{\cdot}8$ Å^{-1} in order to avoid unnecessary addition of statistical noise to the maps. Fig. 2 shows, however, that increase in resolution not only affects features in the bond region (see also Coppens & Lehmann, 1976), but also results in a lower observed $\Delta\rho$ close to the nuclei. Thus, owing to both the uncertainty in the scale factor and the choice of resolution, regions within about 0·3 Å of the nuclei cannot be considered to contain reliable information (Kirfel, Gupta & Will, 1979) and, therefore, these areas are left blank in the deformation density maps. In the region between B and O(1) of Fig. 2, differences in $\Delta\rho$ are due to resolution rather than scaling. In contrast to Coppens & Lehmann (1976), no increase of the bond peak height is observed with increasing resolution. The single-bond peak at low resolution becomes a double peak at higher resolution and in the static deformation density [II(Ca)] (of infinite resolution).

(*a*) *The* BO_2 *chain*

Dynamic deformation density distributions with $K = 1{\cdot}0$ in the plane of the BO_3 triangle are shown in Fig. 3. Figs. 3(*a*) and (*b*) are calculated with equal resolution ($s_{\rm max} = 0{\cdot}8$ Å^{-1}). They demonstrate the following points:

(i) The $\Delta\rho_{\rm dyn}(\mathbf{r})$ maps obtained from the two measurements, *i.e.* after refinements I(Ca) and II(Ca), yield qualitatively the same information. Thus, even the limited data set I allows the derivation of an acceptable deformation density picture, when more accurate displacement parameters are obtained by refinement of the multipole model.

(ii) For the B–O bonds, the quantitative agreement is better than 0·05 e Å^{-3}. Larger differences exist in

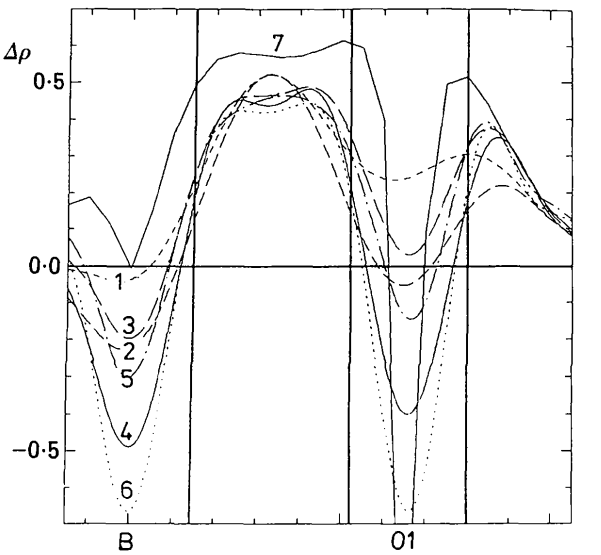

Fig. 2. Linear dynamic deformation density along B–O(1). (1): $K = 1{\cdot}00$; $s_{\rm max} = 0{\cdot}80$ Å^{-1}; (2): $K = 0{\cdot}99$; $s_{\rm max} = 0{\cdot}80$ Å^{-1}; (3): $K = 1{\cdot}00$; $s_{\rm max} = 1{\cdot}00$ Å^{-1}; (4): $K = 0{\cdot}99$; $s_{\rm max} = 1{\cdot}00$ Å^{-1}; (5): $K = 1{\cdot}00$; $s_{\rm max} = 1{\cdot}16$ Å^{-1}; (6) $K = 0{\cdot}99$; $s_{\rm max} = 1{\cdot}16$ Å^{-1}; (7): static deformation density from II(Ca).

the lone-pair regions of the terminal O(1) and the bridging O(2), where charge accumulations appear more pronounced for crystal II. This is understandable considering the superior resolution of data set II which allows a better separation of bonding effects and thermal smearing in the course of the multipole refinement.

Fig. 3(*c*) was calculated after refinement II(Ca^{2+}) showing the deformation density associated with the BO^{2-} ion to be practically independent of the charge of Ca. This result could be expected from the agreement of the refined standard parameters and implies that for the BO_2 part of the structure it suffices to present results of one refinement only.

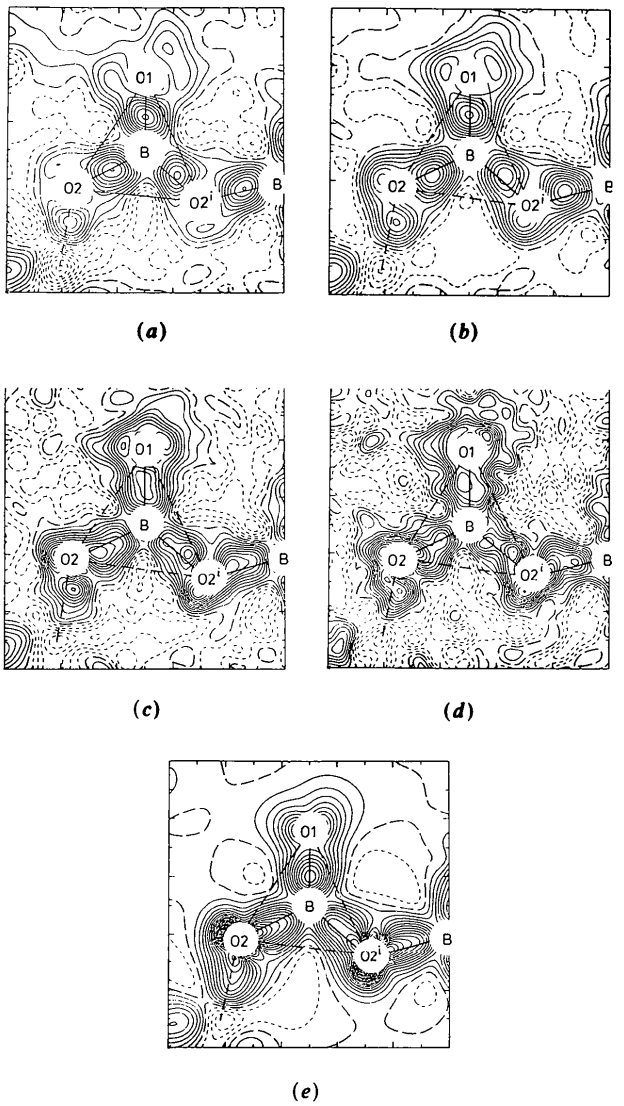

Fig. 3. Dynamic deformation densities in the BO_3 plane. Contours at 0·05 e $Å^{-3}$; zero contour broken, negative contours dashed. (*a*) From I(Ca), $s_{max} = 0{\cdot}80\ Å^{-1}$; (*b*) from II(Ca), $s_{max} = 0{\cdot}80\ Å^{-1}$; (*c*) from II($Ca^{2+}$), $s_{max} = 1{\cdot}00\ Å^{-1}$; (*d*) from II($Ca^{2+}$), $s_{max} = 1{\cdot}16\ Å^{-1}$; (*e*) static deformation density from II(Ca^{2+}).

Table 6. *Interatomic distances* (Å) *and angles* (°) *with e.s.d.'s in parentheses calculated from* II (Ca) [*Also in parentheses corresponding results for* $LiBO_2$ (*Kirfel et al.*, 1983)]

$[BO_2]_\infty$ chain		
B–O(1)	1·3200 (2)	(1·325)
B–O(2)	1·4010 (2)	(1·407)
B–O(2ⁱ)	1·3856 (2)	(1·393)
O(1)–O(2)	2·3205 (2)	
O(1)–O(2ⁱ)	2·4327 (2)	
O(2)–O(2ⁱ)	2·3988 (2)	
O(1)–B–O(2)	117·01 (2)	(117·50)
O(1)–B–O(2ⁱ)	128·07 (2)	(126·57)
O(2)–B–O(2ⁱ)	114·89 (2)	(115·91)
CaO_8 polyhedron		
Ca–O(1ⁱⁱ)	2·3396 (2)	
Ca–O(1)	2·4073 (2)	
Ca–O(2ⁱⁱⁱ)	2·5424 (1)	
Ca–O(1ⁱⁱⁱ)	2·7126 (2)	
O(1)–O(1ⁱᵛ)	2·8107 (2)	
O(1)–O(1ᵛ)	3·0206 (2)	
O(1ⁱⁱ)–O(1ⁱˣ)	3·2588 (2)	
O(1ⁱⁱⁱ)–O(2ⁱⁱⁱ)	2·3205 (2)	
O(1ⁱⁱ)–O(2ⁱⁱⁱ)	3·1255 (2)	
O(1)–O(2ⁱⁱⁱ)	2·8634 (2)	
O(1ⁱᵛ)–O(1)–O(2ⁱⁱⁱ)	105·21 (1)	
O(1ⁱᵛ)–O(1)–O(1ᵛ)	77·99 (1)	
O(2ⁱⁱⁱ)–O(1)–O(1ᵛ)	79·23 (2)	
O(1)–O(2ⁱⁱⁱ)–O(1ᵛⁱⁱ)	75·46 (1)	
O(1)–O(2ⁱⁱⁱ)–O(1ⁱⁱⁱ)	110·66 (1)	
O(1ⁱⁱⁱ)–O(2ⁱⁱⁱ)–O(1ᵛⁱⁱ)	89·28 (1)	

Symmetry codes: (i) $x, \frac{1}{2}-y, z-\frac{1}{2}$; (ii) $\frac{1}{2}+x, y, 1-z$; (iii) $x, y, z-1$; (iv) $\frac{1}{2}-x, -y, z$; (v) $-x, -y, 1-z$; (vi) $-x, -y, 2-z$; (vii) $\frac{1}{2}+x, y, 2-z$; (viii) $x, y, z+1$; (ix) $\frac{1}{2}-x, -y, z-1$.

Figs. 3(*d*) and (*e*) illustrate once more the effect of increasing the resolution of the Fourier synthesis. Besides adding statistical noise to the maps, the bond peaks become elongated into bands of density. The corresponding static deformation density is shown in Fig. 3(*f*). Since $\Delta\rho_{stat}$ represents a filtered deformation density of infinite resolution it should agree best with Fig. 3(*e*), and the comparison indicates in fact that the model was able to accommodate all information contained in the reflection intensities. Correspondingly, a residual density, $[F_o(\mathbf{h}) - F_c^{mult}(\mathbf{h})]$, does not show any significant features and is therefore not shown.

A comparison of the three inequivalent B–O bonds with those in $LiBO_2$ (Table 6) shows the similarity between the two structures. According to Pauling (1948), the B–O bond possesses partial ionic character (electronegativity difference 1·4). It may also be described in terms of resonance between a single and a double bond with the contribution of the latter varying according to the observed bond length. Application of the bond-length–bond-strength relationship (Zachariasen, 1963) yields for the B–O bonds in $Ca(BO_2)_2$ bond strengths of 1·14 for B–O(1), 0·92 for B–O(2), and 0·95 for B–O(2ⁱ). The sum matches well with the B valence number 3.

Dynamic and static deformation density sections from II(Ca) along the three B–O bonds and normal to the plane of the BO_3 triangle are given in Fig. 4. In both types of maps, the B atom possesses a well pronounced quadrupolar deformation [see also Fig. 5(*d*) of the $LiBO_2$ study], in contrast to the O atoms.

The bond-peak heights in $\Delta\rho_{dyn}(\mathbf{r})$ ($s_{max} = 0{\cdot}80$ Å^{-1}) are 0·52, 0·48 and 0·38 e Å^{-3} for B–O(1), B–O(2) and B–O(2^{i}), respectively. In the static deformation density distributions, corresponding values (on the middle of the bonds) are 0·57, 0·50 and 0·40 e Å^{-3}, respectively. These values compare well with the corresponding $\Delta\rho_{stat}$ values in $LiBO_2$ (Kirfel *et al.*, 1983) of 0·60, 0·60 and 0·40 e Å^{-3}, respectively. Thus, in the present study a satisfactory quantitative agreement with $LiBO_2$ is obtained which confirms the order of the bond strengths in terms of $\Delta\rho$. As in $LiBO_2$, this order does not agree well with the bond-length–bond-strength relationship. As in $LiBO_2$, one finds in the BO_3 triangle two apparently strong bonds of rather different lengths associated with the BO_2 anion of metaboric acid, and a weaker bond, B–O(2^{i}), which

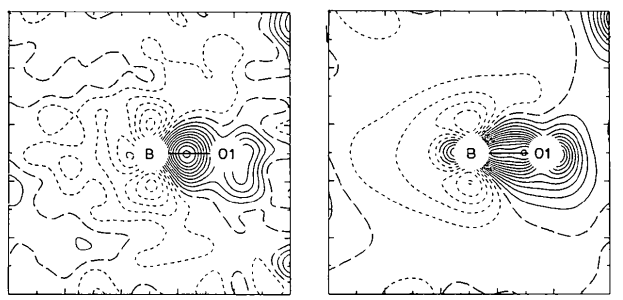

(*a*) (*b*)

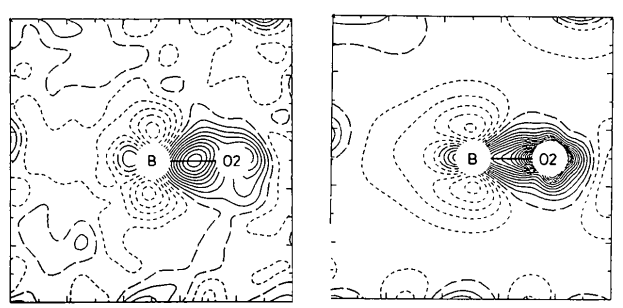

(*c*) (*d*)

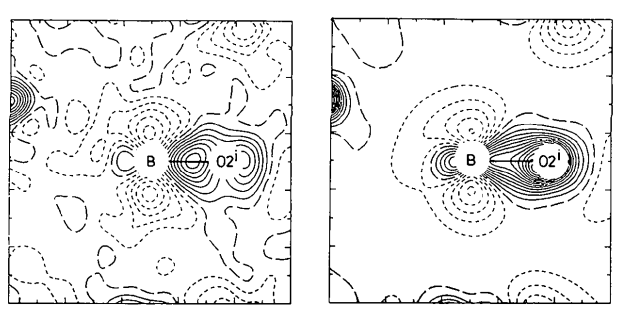

(*e*) (*f*)

Fig. 4. Dynamic and static deformation densities along the B–O bonds and normal to the BO_3 plane from II(Ca^{2+}). Contours as in Fig. 3. (*a*), (*c*), (*e*) dynamic; (*b*), (*d*), (*f*) static.

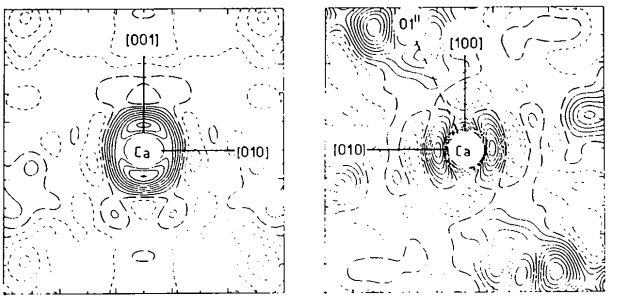

(*a*) (*b*)

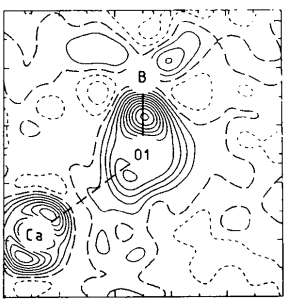

(*c*)

Fig. 5. Dynamic deformation density around Ca. Contours as in Fig. 3. (*a*) Section normal to [100] from II(Ca); (*b*) section normal to [001] from II(Ca); (*c*) B–O(1)–Ca from II(Ca).

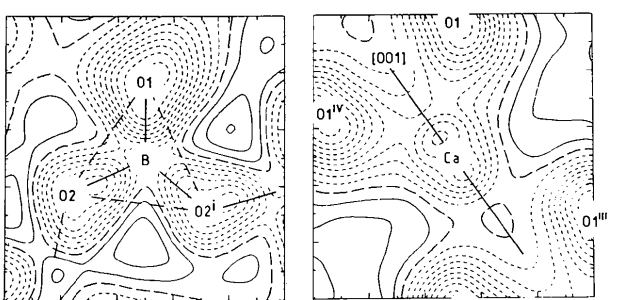

(*a*) (*b*)

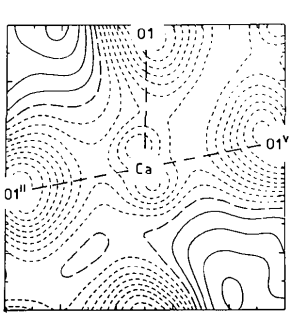

(*c*)

Fig. 6. Deformation potential from II(Ca). Contours at 0·05 e Å^{-1}; zero contour broken, negative contours dashed. (*a*) The BO_3 plane; (*b*) O(1)–Ca–O(1^{iv}); (*c*) O(1)–Ca–O(1^{ii}).

can be interpreted as overlap of an sp^2 hybrid orbital of B and a $2p$ orbital of O giving rise to the polymerization of BO_2 units to endless chains. This aspect is supported by the deformation potential distribution (Fig. 6*a*) showing B–O(1) and B–O(2) associated with lower $\Delta\psi$ than B–O(2^{i}) and thus representing a stable entity within the BO_3 triangle. In analogy to $LiBO_2$, it is the recognition of BO_2 as a unit which suggests this simple model of chemical bonding for the BO_2 chain.

(*b*) *The* Ca *atom*

The average Ca–O distance is 2·500 Å in agreement with the sum of the ionic radii (IR) of $^{viii}Ca^{2+}$ (1·12 Å) and $^{iv}O^{2-}$ (1·38 Å) given by Shannon (1976). However, the position of Ca in the coordination polyhedron (Fig. 1*b*) is shifted by 0·221 Å along [001] from the centroid defined by the eight O atoms towards O(1) and O(1^{iv}). This position and the symmetry of the polyhedron allow a simple estimation of charges associated with O(1) and O(2) using a point-charge model and considering only nearest-neighbour interaction of O^- with Ca^{2+}. Electrostatic attractions on Ca^{2+} are in equilibrium if O(1) carries a charge 40% higher than O(2). As a consequence, the electric field acting on the electrons of Ca is somewhat stronger along [001] than in the opposite direction, and Ca can therefore be expected to possess a small dipole moment parallel to [001].

Dynamic deformation densities in interesting sections through Ca are depicted in Fig. 5 and show the following:

(i) Ca displays charge accumulation in a torus around [100], *i.e.* the atom is flattened parallel to the planes of the BO_3 triangles (Figs. 5*a*,*c*), which may be explained by electrostatic repulsion. From Fig. 5(*c*), one can also observe that the lone-pair density of O(1^{ii}) is directed along the short Ca–O(1^{ii}) bond (2·3396 Å).

(ii) The difference between the deformation densities derived from II(Ca) and II(Ca^{2+}) (Fig. 5*b*) is small. Since the reference density distributions used in the $\Delta\rho$ syntheses are practically the same for both models owing to the diffuse character of the $4s^2$ valence electrons of the free Ca atom. The appearance of $\Delta\rho$ around the Ca position implies a deformation of the 18-electron core (*i.e.* of Ca^{2+}), which scatters far into reciprocal space. This interpretation is supported by the corresponding deformation densities obtained from the multipole refinements with data set I which show a much less pronounced deformation of Ca.

(iii) Additionally to the flattening of Ca, Fig. 5(*a*) shows two deformation density maxima on [001] above and below the Ca position. Both maxima peak at a distance of 0·40 Å from the nucleus, and the peak pointing down is 0·05 e $Å^{-3}$ higher in agreement with the above discussed dipole moment. Correspondingly, all multipole refinements yielded small negative dipole populations $D_{[001]}$ [average value −0·05 (1) e Å].

(iv) Fig. 5 illustrates that not the shortest Ca–O bond, Ca–O(1^{ii}), but Ca–O(1) (2·4073 Å) is the most important bond. O(1) lone-pair density extends into the vicinity of Ca indicating some degree of covalent interaction between O(1) and Ca. This is supported by Figs. 6(*b*), (*c*) showing the deformation potential distribution in two sections through the coordination polyhedron. Ca–O(1) is assoicated with a lower $\Delta\psi$ then Ca–O(1^{ii}). On the other hand, $\Delta\psi$ almost vanishes along the long Ca–O(1^{iii}) bond which emphasizes the directionality of Ca–O interaction within the polyhedron. Thus, as in $LiBO_2$, the terminal O atom appears to form the most important link between the chains and the cations. Again in agreement with $LiBO_2$, O(2) is also polarized towards Ca with the lone-pair peak (Figs. 3*c*,*d*) pointing approximately along O(2)–Ca.

(*c*) *Charge integrations*

In order to assess the charge character of the atoms, spherical charge integrations by direct Fourier summations over the $F(\mathbf{h})_o$ of data set II were carried out according to Sasaki, Fujino, Takeuchi & Sadanaga (1980). The terms for the series-termination corrections were calculated up to $s_{max} = 6{\cdot}0$ $Å^{-1}$ using the isotropic temperature factors of the all-data refinement and the analytical scattering-factor expressions (*International Tables for X-ray Crystallography*, 1974). $F(\mathbf{h})_o$ of reflections flagged as unobserved were substituted by their $F(\mathbf{h})_c$ values. $Z(R)$ curves were calculated with a radial increment of 0·01 Å for Ca and B up to $R = 2{\cdot}0$ Å. By differentiation, dZ/dR, the radial charge density distributions, $4\pi R^2\rho(R)$, are obtained. These are shown together with the respective $Z(R)$ curves in Figs. 7(*a*) and (*b*).

For the Ca atom, Fig. 7(*a*) shows an absolute minimum in the radial charge distribution at $R =$ 1·25 Å. This may be accepted as the 'ionic radius' and is in very good agreement with the crystal radius (CR) for $^{viii}Ca^{2+}$ (1·26 Å) given by Shannon (1976). At this radius, the average electron density is only 0·12 e $Å^{-3}$ ($dZ/dR = 2{\cdot}38$ e $Å^{-1}$), and the number of electrons contained in the sphere is 18·1 (2). Thus, from the integration Ca is found to be twofold positively charged in agreement with chemical expectation. Consequently, each BO_2 unit carries one excess electron, as in the case of $LiBO_2$. Judging from both the charge of Ca and the low electron density at the 'ionic radius' it is evident that the predominant interaction of Ca with its environment is of ionic nature. Fig. 7(*b*) demonstrates for B the well known difficulty in assigning an atomic radius and a charge in the case of considerable covalent bonding. If we take

again the absolute minimum of dZ/dR (2·70 e Å^{-1}, Fig. 7*b*) at $R = 0{\cdot}44$ Å with the average density of 1·11 e Å^{-3} as the criterion for the atomic boundaries in the BO_3 triangle this yields 2·70 e in the B sphere, *i.e.* $B^{2{\cdot}30+}$. This charge estimate is certainly too large and must be attributed to the delocalized character of the sp^2 hybrid orbitals of B, which preclude the assignment of a unique atomic radius. However, it is possible to establish a physically reasonable radius for the $^{iii}B^{3+}$ ion from the sphere containing the two electrons of the *K* shell. Its radius of 0·40 Å can be considered as describing the physically reasonable minimum size of B^{3+}, and comparison with the corresponding B^{3+} 'crystal radius' of 0·15 Å (Shannon, 1976) shows that the latter is severely underestimated. Charges given by the monopole populations from the multipole refinements are omitted since they are only indicative. However, it is worth noting that they also indicate both Ca and B to be positive, while the O atoms show excess charge. Moreover, in all refinements O(1) was found to be more negative than O(2) in agreement with the point-charge model discussed in the previous section.

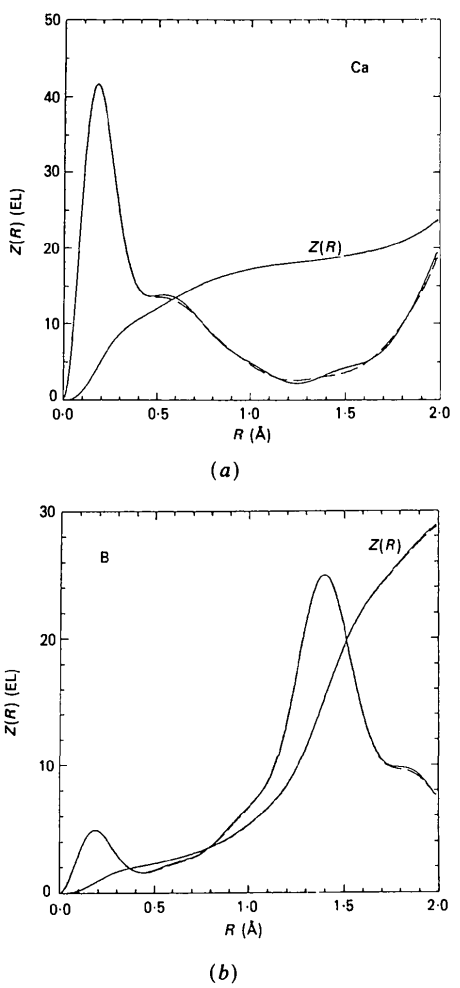

Fig. 7. Spherical charge integration curves $Z(R)$ and radial charge density distributions dZ/dR (on arbitrary scale). Broken curves from calculation with $F(\mathbf{h})_c^{IAM}$. (*a*) For the Ca atom, (*b*) for the B atom.

Concluding remarks

In view of the final agreement indices, the present study is another example of the validity and applicability of the rigid pseudoatom model in electron density investigations. As for $LiBO_2$, the multipole model could be fitted to the measured X-ray diffraction data with *R* values of about 0·01 or less. These values are lower than those obtained from HO refinements. The comparison of the agreement factors and the crystallographic standard parameters derived from the multipole and HO refinements indicates that bond-induced charge redistributions can scatter beyond the generally accepted HO 'cut off' of $s = 0{\cdot}8$ Å^{-1}. This is not surprising since the charge accumulations on the B–O bonds and in the oxygen lone-pair regions as well as the deformation of the Ca cation are well localized. In addition, the multipole method obviously yields more information than the more easily calculated $X - X^{HO}$ synthesis, and should therefore be applied whenever feasible. Data set I may serve as an example. While the limitation to $s = 0{\cdot}8$ Å^{-1} precludes the application of the $X - X^{HO}$ technique, the multipole refinement still yields, at least for the BO_2 chain, qualitatively satisfactory information. Scattering of deformation density features beyond 0·8 Å^{-1} is also shown by $\Delta\rho$ syntheses with data up to 1·0 and 1·16 Å^{-1}. Changing the resolution produces notable alterations of the deformation density pattern, both qualitatively and quantitatively. Series-termination effects become most evident at the atomic positions with the consequence that the well known uncertainties around the nuclei (owing to errors in the scale factor, in the refined standard parameters and in the observations) are *additionally* increased by the choice of the data-resolution limit. This aspect should be considered when comparing electron density results. In the individual case it may then be worth seeking an optimum compromise between the contradictory aims of extracting a maximum of information in the presence of a minimum of statistical noise.

Comparison of the present results of charge density distribution with those of the $LiBO_2$ study on the $s_{max} = 0{\cdot}8$ Å^{-1} level shows good agreement for the BO_2 chain. Bond density values in the regions of the B–O bonds are reproduced within at most 0·1 e Å^{-3}, and the BO_2 anion of metaboric acid can again be recognized as the stable subunit from the deformation density and the deformation potential. Thus, bonding in the BO_2 chains appears to be the same as in $LiBO_2$. It may be described by a polymerization of BO_2. Inspection of the CaO_8 coordination polyhedron with

six corners formed by the terminal O(1) atoms shows that one of the four unique Ca–O bonds can be characterized as preferrred, as was the case for $LiBO_2$. The ranking of the Ca–O bonds according to bond strength and the geometry of the polyhedron correspond to chemical intuition. Thus, the experimental electron density distribution allows the formation of the crystal to be rationalized in terms of moieties $[O(2)BO(1)]^-Ca^{2+}[O(1)BO(2)]^-$, which are joined *via* the free sp^2 hybrid orbitals of the B atoms in a three-dimensional framework. This picture is analogous to the binding model in $LiBO_2$.

Support of this work by the Deutsche Forschungsgemeinschaft is gratefully acknowledged.

References

BECKER, P. & COPPENS, P. (1974). *Acta Cryst.* A**30**, 129-147, 148-153.

BEHM, K. (1976). Dissertation, Univ. Freiburg, Federal Republic of Germany.

CLEMENTI, E. & ROETTI, C. (1974). *Atomic Data and Nuclear Data Tables*, Vol. 14, No. 3-4. New York: Academic Press.

COPPENS, P. & LEHMANN, M. S. (1976). *Acta Cryst.* B**32**, 1777-1784.

CROMER, D. T. & LIBERMAN, D. J. (1970). *Chem. Phys.* **53**, 1891-1898.

EFFENBERGER, H., KIRFEL, A. & WILL, G. (1983). *Tschermaks Mineral. Petrogr. Mitt.* **31**, 151-164.

HAMILTON, W. C. (1965). *Acta Cryst.* **18**, 502-510.

HEHRE, W. J., DITCHFIELD, R., STEWART, R. F. & POPLE, J. A. (1970). *J. Chem. Phys.* **521**, 2769-2773.

International Tables for X-ray Crystallography (1974). Vol. IV. Birmingham: Kynoch Press. (Present distributor D. Reidel, Dordrecht.)

KIRFEL, A., GUPTA, A. & WILL, G. (1979). *Acta Cryst.* B**35**, 2291-2300.

KIRFEL, A. & WILL, G. (1980). *Acta Cryst.* B**36**, 2881-2890.

KIRFEL, A. & WILL, G. (1981). *Acta Cryst.* B**37**, 525-532.

KIRFEL, A., WILL, G. & STEWART, R. F. (1983). *Acta Cryst.* B**39**, 175-185.

MAREZIO, M., PLETTINGER, H. A. & ZACHARIASEN, W. H. (1963). *Acta Cryst.* **16**, 390-392.

PAULING, L. (1948). *The Nature of the Chemical Bond.* Ithaca, New York: Cornell Univ. Press.

SASAKI, S., FUJINO, K., TAKEUCHI, Y. & SADANAGA, R. (1980). *Acta Cryst.* A**36**, 904-915.

SHANNON, R. D. (1976). *Acta Cryst.* A**32**, 751-767.

STEVENS, M. D. & COPPENS, P. (1976). *Acta Cryst.* A**32**, 915-917.

STEWART, R. F. (1976). *Acta Cryst.* A**32**, 565-574.

STEWART, R. F. (1979). *Chem. Phys. Lett.* **65**, 335-342.

STEWART, R. F. & SPACKMAN, M. A. (1981). *VALRAY Users Manual.* Preliminary Draft. Department of Chemistry, Carnegie-Mellon Univ., Pittsburgh, PA 15213.

WAL, R. J. VAN DER, VOS, A. & KIRFEL, A. (1987). *Acta Cryst.* B**43**, 132-143.

ZACHARIASEN, W. H. (1963). *Acta Cryst.* **16**, 385-389.

ZACHARIASEN, W. H. & ZIEGLER, G. E. (1932). *Z. Kristallogr.* **83**, 354-356.

Acta Cryst. (1987). B**43**, 343-346

Electron-Microscopic Study of the Structure of Metastable Oxides Formed in the Initial Stage of Copper Oxidation. IV. Cu_4O-S_1 and Cu_4O-S_2

BY R. GUAN

Laboratory of Atomic Imaging of Solids, Institute of Metal Research, Academia Sinica, Shenyang, People's Republic of China

H. HASHIMOTO

Department of Applied Physics, Osaka University, 2-1 Yamadaoka, Suita, Osaka 565, Japan

K. H. KUO

Laboratory of Atomic Imaging of Solids, Institute of Metal Research, Academia Sinica, Shenyang, People's Republic of China

AND T. YOSHIDA

Department of Applied Physics, Osaka University, 2-1 Yamadaoka, Suita, Osaka 565, Japan

(*Received* 9 *December* 1986; *accepted* 10 *March* 1987)

Abstract

Besides Cu_4O, Cu_8O and $Cu_{64}O$ reported previously, two superstructures of the metastable copper oxides Cu_4O, called Cu_4O-S_1 and Cu_4O-S_2, have been observed by high-resolution electron microscopy in an early stage of oxidation of Cu together with Cu_4O. The atom positions of Cu and O have been determined by comparison of the observed structure images with simulated ones calculated using the theories of electron diffraction and image formation. Some O atoms in the superstructures occupy octahedral positions of the face-centered cubic lattice of Cu, while the others remain in tetrahedral positions

0108-7681/87/040343-04$01.50